Journal of Alloys and Compounds 622 (2015) 687–694

Contents lists available at ScienceDirect

Journal of Alloys and Compounds

journal homepage: www.elsevier.com/locate/jalcom

Investigations on electrical conductivity and dielectric properties of Na doped ZnO synthesized from sol gel method

Asma Tabib [a], Nasr Sdiri [a], Habib Elhouichet [a,b,*], Mokhtar Férid [a]

[a] Laboratoire de Physico-Chimie des Matériaux Minéraux et leurs Applications, Centre National de Recherches en Sciences des Matériaux, B.P. 95 Hammam-Lif, 2050, Tunisia
[b] Département de Physique, Faculté des Sciences de Tunis, University Tunis El Manar, Tunis 2092, Tunisia

ARTICLE INFO

Article history:
Received 7 October 2014
Accepted 17 October 2014
Available online 6 November 2014

Keywords:
ZnO
Impedance spectroscopy
Ionic conductivity
Dielectric relaxation
Electrical modulus

ABSTRACT

Na doped ZnO nanoparticles (NPs) were elaborated by sol gel technique. The X-ray diffraction patterns show that the peaks are indexed to the hexagonal structure without any trace of an extra phase. Electric and dielectric properties were investigated using complex impedance spectroscopy. The impedance spectra were analyzed in terms of equivalent circuits involving resistors, capacitors and constant phase elements (CPE). The contribution of grain boundary resistance to the total resistance of the system is remarkable. The AC conductivity increases with temperature following the Arrhenius law, with single apparent activation energy for conduction process. The frequency dependence of the electric conductivity follows a simple power law behavior, in according to relation $\sigma_{AC}(\omega) = \sigma(0) + A\ \omega^s$, where s is smaller than 1. The analysis of dc conductivity indicates that the conduction is ionic in nature. The study of its variation, at fixed temperature, with Na content shows sharp decrease which is explained by the formation of Na_{Zn} acceptor. It was found that the dc conductivity reaches its minimum value for critical Na concentration of 1.5% at which the conductivity is estimated to be of p-type. Impedance and modulus study reveals the temperature dependent non-Debye type relaxation phenomenon. Dielectric studies revealed a promising dielectric properties (relatively high ε' at low frequencies and low loss at high frequencies). In the low-frequency region, the values of M' tends to zero suggesting negligible or absent electrode polarization phenomenon. The frequency dependent maxima in the imaginary modulus are found to obey to Arrhenius law.

© 2014 Elsevier B.V. All rights reserved.

1. Introduction

For the last decades, there has been increasing interest for oxides because of their wide variety of applications. Belonging to this family, zinc oxide (ZnO) is an n-type semiconductor [1,2] with a direct large band gap of 3.37 eV [3,4] which is considered as promising candidate for optical and optoelectronic applications in nanoscale devices [5,6]. It is used as a transparent electrode in solar cells [7], chemical and gas sensors [8], spintronic devices [9], and light emitting diodes [10]. Impedance spectroscopy (IS) is considered to be a powerful tool of analyzing the electrical properties of polycrystalline material. By changing the applied frequency of the system, different contributions of the electrodes, grain boundaries and individual grains can be distinguished [11,12], whereby, the conductivity of material can be determined via charge transport of the grain and through the grain surface as well as via barriers formed on crystallite boundaries. Thus, by investigating the impedance spectroscopy, we can study the charge transport mechanism that contributes to the conductivity of material.

The electrical conductivity generally consists of both ionic and electronic conduction. Conductivity in alkali modified zinc oxide is generally attributed to the transport of alkali cations and is called ionic [13]. But in the presence of transition metal ions, we speak about electronic conductivity which is governed by the following mechanism [14–16]: during doping, defects are created in the band gap and are filling some energy level [17]. Around these levels, the charge carriers are localized and creating a small polaron [18–20]. The conduction can take place by transfer of electrons between the localized states [21]. As it is reported in the literature, the presence of more than one valance states on transition metal ion suggests that polaronic conduction is attributed to a hopping mechanism of electrons from low valence state to high valance one [22–24]. The ac conductivity study at variable frequencies and temperatures give useful information about the mobile ion diffusion and short time phenomena due to local motion of mobile ions [25].

* Corresponding author at: Département de Physique, Faculté des Sciences de Tunis, University Tunis El Manar, Tunis 2092, Tunisia.
E-mail address: habib.elhouichet@fst.rnu.tn (H. Elhouichet).

http://dx.doi.org/10.1016/j.jallcom.2014.10.092
0925-8388/© 2014 Elsevier B.V. All rights reserved.

Despite the number of papers already published on the synthesis of ZnO powders, the effects of alkali-metal on the dielectric characteristics of the grains and grain boundaries, especially the type and activation energies of the characteristic relaxation processes in the doped and undoped ZnO crystals, are still not well developed. New approach for preparing sodium doped ZnO by simple process with low cost and easy preparation, called sol gel technique, is adopted in the present study. Our research group has shown that sol gel ZnO is with high crystalline quality and good optical performances [26,27].

The choice of sodium as dopant is motivated by its ability as dopant for producing p-type ZnO, its abundance and its low cost comparing to other alkali metals as well as its wide field of application. However, the Na-doping behavior and conduction mechanisms are still unclear. There are so many literatures reported on structural, optical and electric properties of Na doped ZnO nanostructures [28–30]. But, to the best of our knowledge, there is no report or published paper devoted to dielectric properties of ZnO NPs doped with Na^+ ions. Therefore, we motivated to study the electrical conductance and frequency dependent dielectric properties of Na doped ZnO NPs prepared by the sol–gel method, as it is a least explored area till now.

2. Experimental

2.1. Preparation of ZnO NPs

The precursors used for the synthesis of sol gel ZnO:Na nanoparticles are: zinc acetate ($Zn(O_2CCH_3)_2(H_2O)_2$), sodium acetate (CH_3COONa) and citric acid ($C_6H_8O_7$), used as zinc source, sodium source and stabilizer, respectively. All chemical materials were prepared from Sigma–Aldrich Company, and were applied without further purification.

Zinc acetate (1.23 g) and citric acid (5 g) are dissolved in 250 ml of bi-distilled water under magnetic stirring. An adequate amount of sodium acetate dopant is added to the above solution with different concentrations (where the molar ratio of Na to Zn is 0.5%, 1%, 1.5%, and 3%). The solutions were vigorously stirred for 1 h by means of a magnetic stirrer to yield a clear and homogeneous solution. Then, they were dried at 80 °C for 7 days in an oven. The dried gels were ground to make fine powders. The dried powders were further calcined at 300 °C for 2 h. After grinding, they undergo a second calcination at 600 °C to obtain crystalline phase. Finally, Na doped ZnO NPs were obtained.

2.2. Experimental characterization

X-ray diffraction (XRD) patterns were obtained at room temperature with a Philips X'Pert system, using Cu Kα radiation ($\lambda = 1.54056$ Å), at 40 kV and 100 mA; the diffractometer settled in the 2Θ range from 3° to 70° by changing the 2Θ with a step size of 0.02°. Absorption spectra were recorded using a Perkin Elmer Lambda UV/Vis 900 spectrophotometer. The wavelength range was 250–900 nm with a step of 2 nm. The reflectance spectra were collected using the Angle Absolute Universal Reflectance Accessory (URA) purchased from Perkin Elmer. Dielectric properties were assessed by measuring complex impedance using an impedance analyzer (Agilent 4294A) in the 40 Hz to 6 MHz frequency range at room temperature.

3. Results and discussion

3.1. X-ray diffraction analysis

Fig. 1 shows the XRD patterns of the pure and Na-doped ZnO NPs. As seen from this figure, these NPs are polycrystallines. The peak indexing was well matched with hexagonal structure of ZnO using the standard data (JCPDS-36-1451) [Joint Committee on Powder Diffraction Standards, Powder Diffraction File No. 36-1451]. Moreover, the XRD patterns show narrow and sharp diffraction peaks indicating good crystalline quality of the samples. We notice also that there are no peaks corresponding to Na_2O crystals or other Na phases which indicates the incorporation of Na dopant into the ZnO lattice as substitutional ion.

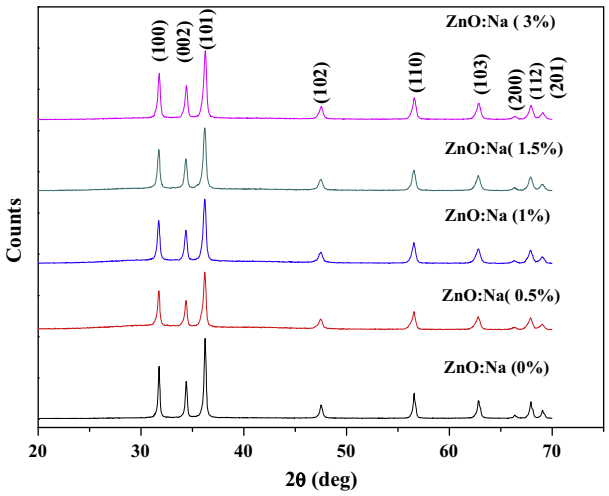

Fig. 1. X-ray diffraction pattern of Na doped ZnO NPs.

3.2. Impedance spectroscopy

3.2.1. Electric study

3.2.1.1. Impedance spectra. Fig. 2 shows the Cole–Cole plots of the pure and Na doped ZnO NPs at different temperatures. Theoretical curve fitting and experimental data are measured. Well-defined semicircles either passing through or closed to the origin were obtained at different temperature and for different percentages of doping. For all samples, the high frequency impedance data are represented in the complex plane by a single semicircle, confirming that they are homogenous and single-phased. These semicircles are most commonly depressed and their centers lie below the Z' axis showing a relaxation of non Debye in all cases [31,32]. The equivalent electrical circuit of the samples is well described by the parallel of capacitance and resistance. Because of the detected impedance decentralization, the capacitor may be replaced by a constant phase element (CPE). The total impedance of the circuit is given by:

$$Z^* = Z' + jZ'' = \left[\frac{1}{R_b} + \frac{1}{Z^*_{CPE}}\right]^{-1} \quad (1)$$

where the impedance of the CPE is defined via [33,34]:

$$Z^*_{CPE} = \frac{1}{A_0(j\omega)^n} \quad (2)$$

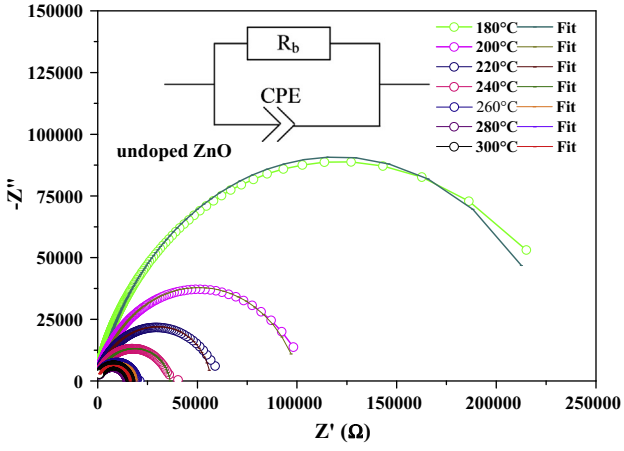

Fig. 2. Experimental and theoretical impedance diagrams of the undoped ZnO with inset the corresponding equivalent circuit.

where j is the imaginary unit ($j^2 = -1$) and ω the angular frequency ($\omega = 2pf$, f is the frequency), A_0 a constant independent of frequency and in F cm^{-2} S^{n-1} [35], and n is a dimensionless parameter ranging between zero and unity and determining the degree of deviation from an exact semicircle [36]. The bulk resistance R_b is the cross of axis with the impedance curve. These semicircles have been fitted by the software ORIGIN6.0 based on the following relationships.

$$ReZ^* = \frac{R_b(1 + R_b A_0 \omega^n \cos(\frac{\pi n}{2})}{1 + 2R_b A_0 \omega^n \cos(\frac{\pi n}{2}) + (R_b A_0 \omega^n)^2} \quad (3)$$

$$ImZ^* = \frac{(R_b)^2 A_0 \omega^n \sin(\frac{\pi n}{2})}{1 + 2R_b A_0 \omega^n \cos(\frac{\pi n}{2}) + (R_b A_0 \omega^n)^2} \quad (4)$$

Nyquist plots reported in Figs. 2 and 3 show a good agreement between simulated and experimental data indicating that the proposed equivalent circuit describes well the electrical properties of the sample. The extract parameters for the circuit elements are collected in Table 1. The capacitance values are found to be 10^{-10} F cm^{-2} S^{n-1}, proving that the observed semicircles represented the grain boundary response of the system [37]. In a study conducted by Fan and Freer [38], the effects of Ag doping on the electrical properties of ZnO varistor compositions were studied. They found that both the grain and grain boundary resistances increase with the addition of Ag, and proposed that Ag^+ could substitute Zn^{2+} and acts as an acceptor in ZnO. Due to the formation of Ag acceptors, the grain resistance is increased. They proposed that Ag^+ may occupy the grain boundary sites, and consequently, the grain boundary resistance is increased. Besides, due to the charge difference and ionic radius between Ag^+ and Zn^{2+}, the substitution of Zn by Ag at the lattice sites would result in the formation of Ag acceptors, the formation of acceptors is usually accompanied with an increase in grain resistance. Fan and Freer [38] suggested also that Ag^+ may behave like other monovalent dopant ions (e.g. Na^+ and K^+) which have the ability to occupy both the lattice and interstitial sites (i.e. amphoteric dopants). Basing on these results and taking into account that Na^+ (0.102 nm) has so much ionic radius than Zn^{2+} (0.074 nm), we can explain the increase in the resistance in our samples by the existence of Na^+ in the lattice that may substitute Zn^{2+} and forming Na acceptors. Previous studies have found that monovalent dopants, such as K^+ and Na^+, act as amphoteric dopants [39,40]. Recently, Kuo et al. [41] have prepared various amounts of silver particles mixed with zinc oxide powder and subsequently co-fired at 800–1200 °C, they found that Ag^+ is likely to act as an amphoteric dopant and occupy both the lattice and interstitial sites since Ag solutes are not acceptors in ZnO. Ag^+ would preferentially choose to sit in the vicinity of grain boundaries due to its large ionic radius.

Table 1
Fitting values of equivalent circuit elements for different samples at temperature $T = 400$ °C.

Percentage of doping (%)	R_b (Ω)	A_0 (10^{-10} F cm^{-2} S^{n-1})	N
0	216711	1.8	0.8
0.5	435872	3.5	0.78
1	390449	3	0.79
3	559757	1.08	0.86

Also, the dc electrical conductivity of the Li-doped ZnO was lower than that of the undoped ZnO, and both the grain and grain boundary electrical conductivity were lower in the Li-doped ZnO than in the undoped ZnO, because the Li doping causes the formation of acceptor levels in ZnO [42].

Table 1 shows that the value of n is practically constant for the after doping with 0.5% and 1% but it increases for 3% doping indicating that the samples behaves almost like a capacitor but with lower capacitance.

3.2.1.2. Dc conductivity. The dc conductivity is expressed in terms of Z_0, which is defined by the interception of the real axis with the lowest-frequency curve. It is given by the following expression:

$$\sigma_{dc} = \frac{e}{SZ_0} \quad (5)$$

where S is the sample area and e is the sample thickness.

In Fig. 4, we present the dc conductivity, obtained from the complex impedance plot, as a function of 1000/T. The dc conductivity, more preciously, the product of the dc conductivity and temperature, often follows an Arrhenius formula:

$$\sigma_{dc} \cdot T = \sigma_0 \exp\left(-\frac{E_a}{K_B T}\right) \quad (6)$$

where σ_0 is a prefactor, E_a is dc activation energy and k_B is the Boltzmann constant. The values of activation energy E_a can be deduced from the slopes of the lines fitting the curves $\sigma_{dc} \cdot T$ versus $\frac{1000}{T}$.

From the plot, it is observed that the conductivity of the ZnO samples was found to increase linearly with increasing temperature and Na percentage. We notice also that only one slope is apparent over an entire set of measurements being further evidence of single conduction mechanism activation.

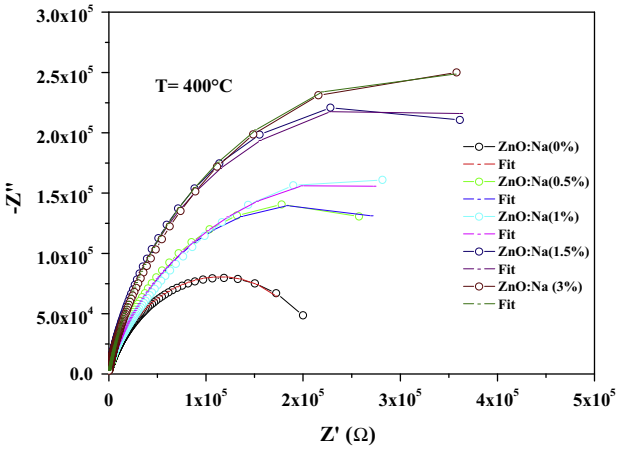

Fig. 3. Experimental and theoretical impedance diagrams of ZnO:Na NPs at $T = 400$ °C.

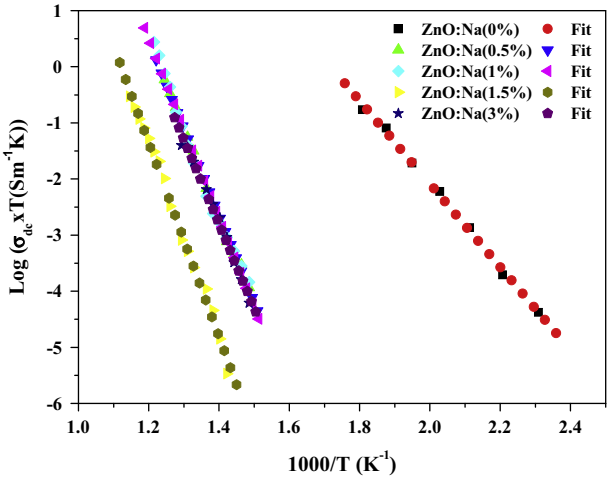

Fig. 4. Arrhenius relation of Log(σ_{dc} T) versus 1000/T for all samples.

The variation of activation energy with Na content is represented in Fig. 5. It is clearly seen that conductivity activation energy of the ZnO is lower than those of the Na doped ZnO NPs. Besides, the obtained values are so high than those reported in other papers [43,44]. However, these values are in the same range (1.17–1.29 eV) than those reported for ZnO doped with Fe which is known to create acceptor levels in ZnO band gap [45]. The higher values of activation energy indicate the low mobility of ions in the sample and are mainly determined by the intrinsic defects which will induce an ionic diffusion [46]. The increase of the activation energy with the amount of Na^+ content indicates that these ions create deep energy levels in the band gap of ZnO and act as acceptors which cause the fall of the Fermi level. Similar behavior has been reported for ZnO:Co [47].

The fluctuation of σ_{dc} with Na content at fixed temperature $T = 400$ °C was illustrated in Fig. 5. The reduction of the conductivity with increase in Na concentration between 0.5% and 1.5% is caused by the segregation of excess Na atoms in the grain boundaries, acting as electrons traps and forming a Schottky barrier. The feature inhibits their electrical activity as doping atoms. The same behavior of the reduction in the conductivity after a critical doping level is reported by many authors with different doping atoms [48,49]. Also, Na atoms substitute Zn atoms in ZnO NPs, and the formation of Na_{Zn} acceptor is at the origin of the decrease of the conductivity which may p-type for ZnO:Na1.5%.

The enhancement in the conductivity for Na concentration above 1.5% can be interpreted by the increase in the number of the free charge carriers coming from the ions Na^+ incorporated in the substitutional site in the presence of an ionic diffusion [50]. In fact, more oxygen interstitials might be produced because Na interstitials increase as the Na doping concentration is dramatically enhanced which might lead to an increase of the electron concentration [51,52].

3.2.1.3. Ac conductivity. The frequency variation of ac conductivity, at various temperatures is shown in Fig. 6(a). The nature and the mechanism of the conductivity dispersion in solids are generally analyzed using Jonscher's power law [53,54]:

$$\sigma_{ac} = \sigma_{dc} + A\omega^s \quad (7)$$

where σ_{dc} is the dc conductivity in particular range of temperature and frequency, A is a temperature dependent parameter and s is the temperature dependent exponent in the range of $0 \leqslant s \leqslant 1$ [55,56]. The exponent s represents the degree of interaction between mobile ions with the lattices around them while the prefactor exponent A determines the strength of polarizability [57]. The detailed analysis of σ_{ac} of ZnO suggests that the power law is obeyed. It is confirmed

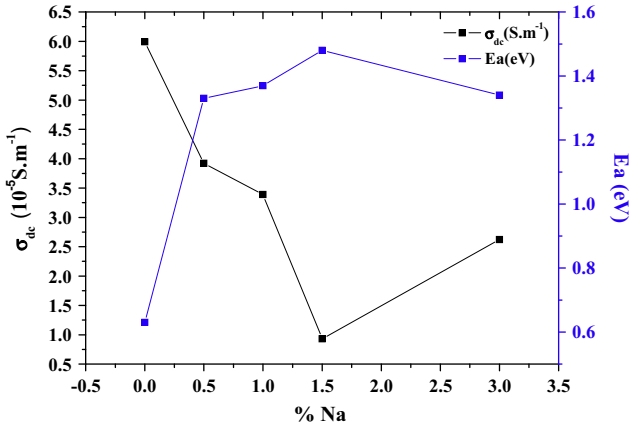

Fig. 5. Variation, at $T = 400$ °C, of σ_{dc} and E_a with Na content.

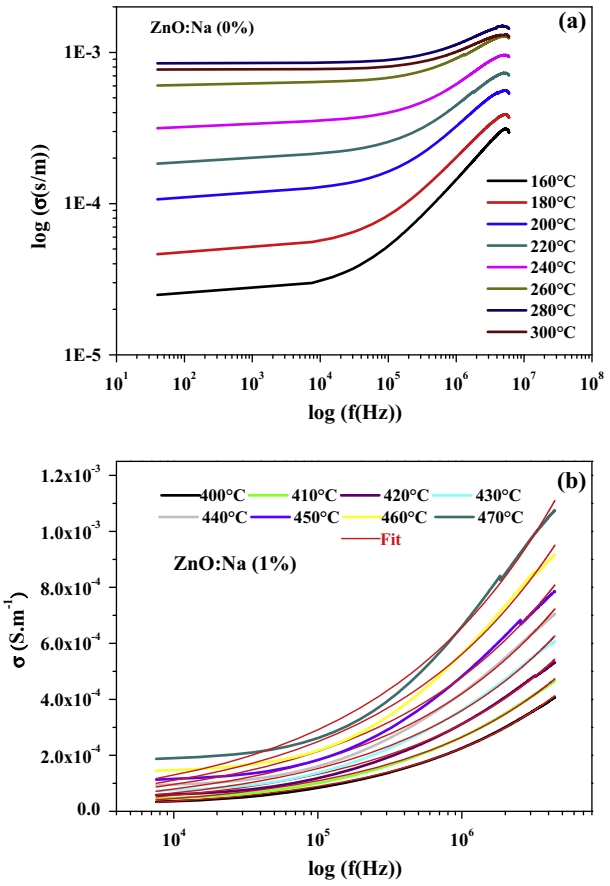

Fig. 6. (a) Variation of the ac conductivity σ_{dc} of undoped ZnO versus frequency (f) at different temperatures and (b) theoretical fit and experimental data of σ_{ac} for the sample ZnO:Na (1%).

by the typical fit of the above equation to the experimental data in Fig. 6(b). At high frequencies, the conductivity shows dispersion attributes to the ac conductivity whereas the frequency independent plateau region at low frequencies corresponds to dc conductivity of the material. This behavior is typical of ionic conductors [58]. The temperature at which grain resistance dominates over grain boundary resistance is marked by a change in slope of ac conductivity with frequency. The frequency at which the change of the slope takes place is known as the critical or hopping frequency. Moreover, the charge species that have been cumulated at the grain boundaries have sufficient energy to jump over the barrier on increasing temperature [59,60].

The observed behavior is in general in agreement with the prediction of the jump relaxation model [61]. According to this model, at low angular frequencies an ion jumps from one site to its neighboring vacant site successfully contributing to dc conductivity. The observed conductivity relaxation at high angular frequencies can be due to the probability of the correlated forward–backward hopping together with the relaxation of the ions.

From the theoretical fit, we can obtain the parameters σ_{dc} and s and evaluate their variation with temperature and doping. The exponent s can be expected if the polarizability of involved material depends on the energy barrier for a simple hopping process between two sites [62]. Some reports, involving hopping models, indicate that s varies in the range from 0.6 to 1 and indicate that it depends on temperature and frequencies [36]. In order to identify the conduction mechanism in our electrolyte system, the exponent s is plotted as a function of temperature as depicted in Fig. 7. For ZnO:Na(0.5%) and ZnO:Na(1%) samples, it was found that

exponent s, calculated at higher frequencies, slightly decreases from 0.43 to 0.32 with increasing temperature from 673 K to 743 K. This behavior has been previously predicted by correlated barrier hopping (CBH) model [63] and overlapping large polaron tunneling (OLPT) for a reduced polaron radius model [64,65]. The CBH model describes charge carriers hop between sites over the potential barrier separating them rather than tunneling through the barrier. This model gives the exponent s parameter as:

$$s = 1 - \frac{6K_BT}{E_a} \tag{8}$$

where k_B is Boltzmann constant and E_a is optical band gap.

3.2.2. Dielectric study

3.2.2.1. Permittivity and loss studies. The complex dielectric constant ε^* deduced from Z′ and Z″ is given by:

$$\varepsilon^* = \varepsilon' - j\varepsilon'' = \frac{1}{j\omega C_0(Z' + jZ\prime\prime)} \tag{9}$$

$$\varepsilon' = -\frac{Z''}{\omega C_0(Z'^2 + Z''^2)} \tag{10}$$

$$\varepsilon'' = -\frac{Z'}{\omega C_0(Z'^2 + Z''^2)} \tag{11}$$

where ε' and ε'' are the real part known as dielectric constant and the imaginary part known as dielectric loss of the complex permittivity respectively. They depend on frequency. $C_0 = \frac{\varepsilon_0 A}{e}$ is the capacitance of the empty cell (ε_0 is the permittivity of the vacuum (8.854×10^{-12} F m^{-1}), A is the cross-sectional area of the flat surface of the pellet ($78.5 \cdot 10^{-6}$ m^2) and e is its thickness (10^{-3} m)). Z′ is the real part of impedance and Z″ is its imaginary part. From values of the dielectric constant we can determine the loss given by [66]:

$$tan\delta = \frac{\varepsilon''}{\varepsilon'} \tag{12}$$

As observed from Fig. 8(a), the dielectric constant increases with increasing temperature and decreases with increasing frequency. This behavior indicates a Debye-type dielectric dispersion [67]. On the other hand, the usual behavior of increasing ε' with temperature may be due to a decrease in bond energies and dissociation of more alkali cations from their sites, and the consequent increase in diffusion or oscillation process through the zinc oxide matrix [68].

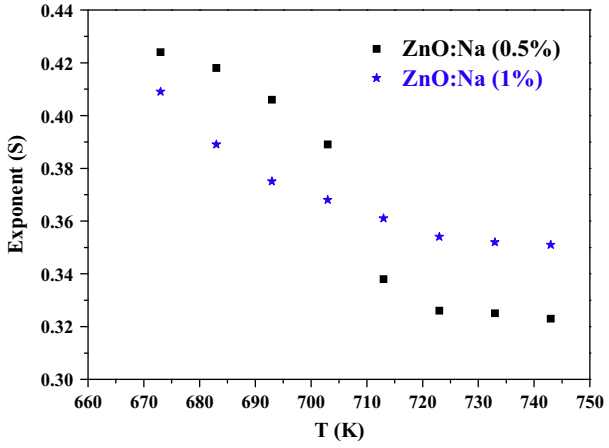

Fig. 7. Variation of the exponent parameter s with temperature for the ZnO samples doped 0.5%Na and 1%Na.

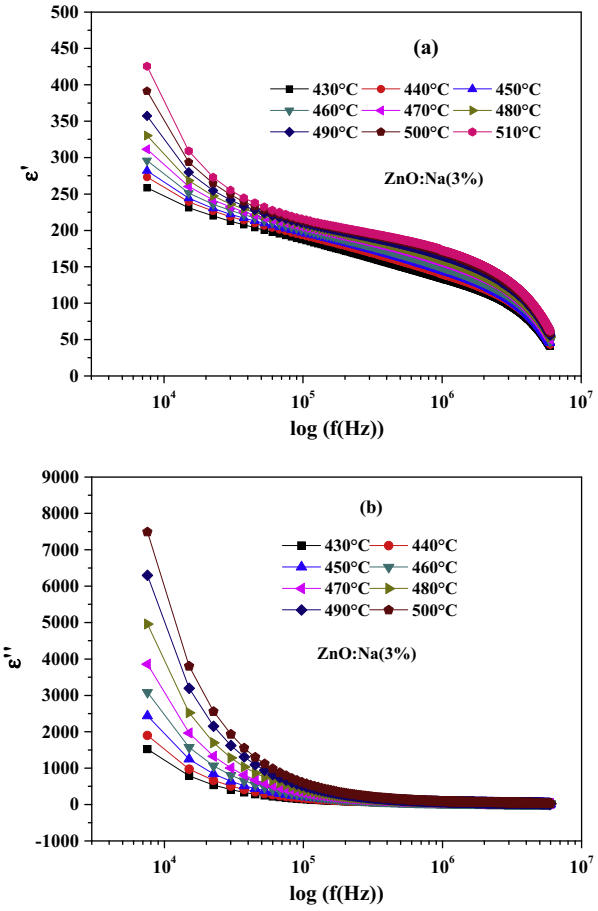

Fig. 8. The frequency dependence curves of dielectric constant ε' (a) and conduction loss ε'' (b) of ZnO:Na (3%) at different temperatures.

The change in ε' is significant at low frequencies for all samples; this may be attributed to the polarizability arising from the contribution of all the existing components. Besides, this later records relatively higher values that were explained by the presence of grain or interphase boundaries [69]. The decrease in ε' with the frequency of the investigated samples may be attributed mainly to the decreasing number of dipoles which contribute to polarization or either to the inability of dipoles to rotate rapidly leading to a lag between frequency of oscillating dipole and that of applied field [70]. In addition, at higher frequency, ε' approaches a constant value which probably results from rapid polarization processes occurring [71].

The variation of the imaginary part of the permittivity with frequency is shown in Fig. 8(b). In the present case, the conduction losses predominate at lower frequencies and hence at all temperatures the imaginary part of the permittivity shows frequency dependence. Also, ε'' is found to increase with temperature and dielectric loss peak has not been observed. However, in ionically conducting materials, at low frequencies there is an unavoidable electrode polarization effects and the conduction losses are rather high [72].

Fig. 9 shows the variation of the dielectric loss with frequency. Accordingly, for all samples the dielectric loss at low and moderate frequency takes relatively high values. This is due to the contribution of both ion jump and conduction loss or to the presence of all types of polarizations electronic, ionic, orientation, space charge polarization, etc. [73]. With the increase in applied field frequency, the ions are increasingly unable to respond to the field and the dielectric loss decreases. This decrease can be attributed to the

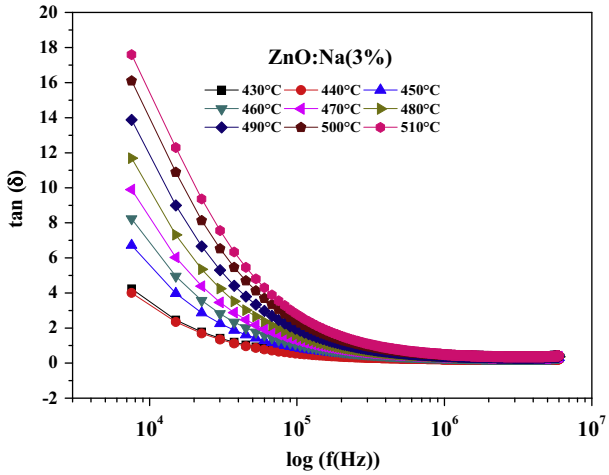

Fig. 9. Variation of the dielectric loss (tanδ) versus frequency for the sample ZnO:Na(3%) at different temperatures.

reduction of the diffusion of the ions in matrix with increasing of the frequency [74] and the reached low value of dielectric loss indicates that the produced powders are of good quality [75]. The low dielectric loss at higher frequency of the samples is of fundamental use for nonlinear optical materials in their application [76]. In fact, the result is in concordance with the index values already found above.

3.2.2.2. Modulus analysis. The complex electrical modulus formalism has been used in the analysis of the electrical properties because it gives the main response of the bulk of sample crystal and is particularly suitable to extract phenomena such as electrode polarization and conductivity relaxation times. It also emphasizes the grain boundary conduction process and is useful for separating spectral components of materials having similar resistances but different capacitances. The complex electric modulus can be represented by the following expression.

$$M^* = M' + jM'' = \frac{1}{\varepsilon^*} = jC_0\omega Z^* \tag{13}$$

We have measured both resistive (real part) and reactive (imaginary part) of complex impedance spectroscopic parameters. From the use of these data in various frequency ranges, we have calculated different material parameters from the following relations:

$$M' = \omega C_0 Z'' \tag{14}$$

$$M'' = \omega C_0 Z' \tag{15}$$

It should be noted that M', the real part of the modulus represented in Fig. 10(a) increases with increasing temperature and at sufficiently high temperature reaches a plateau which corresponds to the limiting value of M'. In the low-frequency region, M' tends to zero suggesting negligible or absent electrode polarization phenomenon [77]. A continuous dispersion on increasing frequency may be due to the short-range mobility of charge carriers. The imaginary part of M^*, as a function of angular frequency is visualized in Fig 10(b), it shows a slightly asymmetric peak at each temperature. The peak shifts toward higher angular frequencies with increasing temperature. This behavior suggests that the dielectric relaxation is thermally activated in which hopping mechanism of charge a carrier dominates intrinsically. The asymmetric broadening of the peak indicates the spread of relaxation with different time constant, and hence, relaxation in the material is of non-Debye type [78].

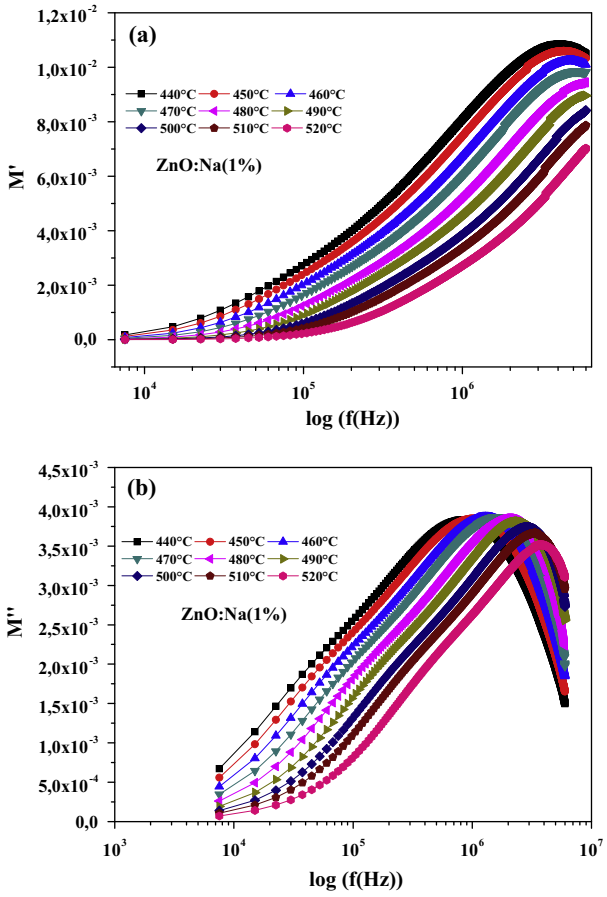

Fig. 10. The frequency dependence of M' (a) and M'' (b) at different temperatures for the sample ZnO:Na (1%).

Such spread is possibly due to the coupling of individual relaxation processes, indeed one site needs to relax before the other can do so [79].

The peak frequency M''_{max} helps to evaluate relaxation time (τ) using a relation $\omega_{max}\tau = 1$. The variation of τ as a function of temperature is shown in Fig. 11. The variation of τ as a function of inverse of absolute temperature appears to be linear which follows the relation $\tau = \tau_0 \exp(-E_a/K_BT)$, where τ_0 is the pre-exponential factor, E_a is the activation energy, k_B is the Boltzmann constant

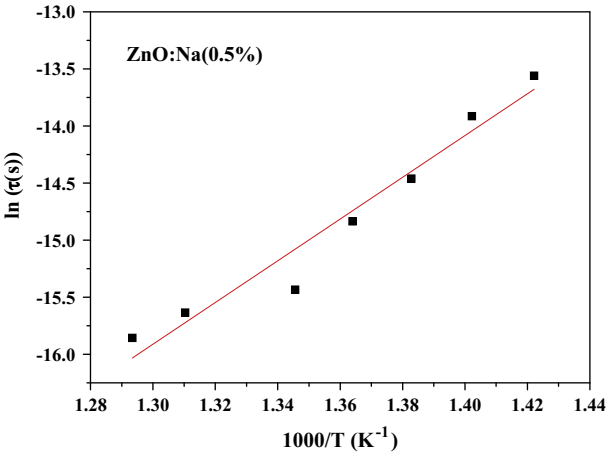

Fig. 11. Variation of relaxation time Lnτ with inverse of temperature 1000/T.

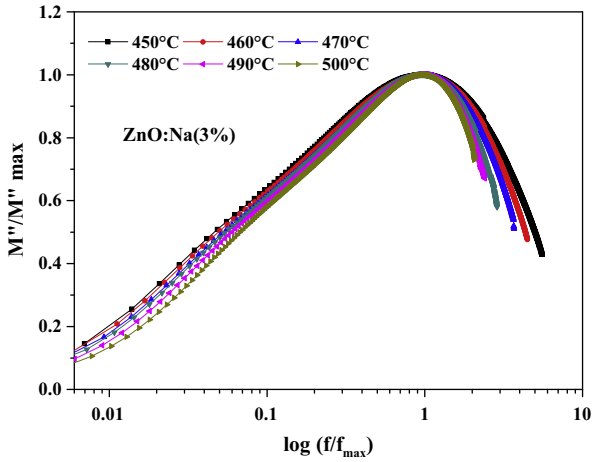

Fig. 12. Curves M''/M''_{max} versus f/f_{max} for the sample ZnO:1%Na at different temperatures.

and T is the absolute temperature. The activation energy E_a obtained from the linear fit is 1.57 eV. This value is different from that found from the plot $\ln(\sigma_{dc}T)$ versus $1000/T$ confirming the hypothesis previously stated: a non-statistic distribution of the cations in the lattice induces a random conductivity, thus the relaxation of dipoles occurs itself randomly. Indeed, the response of sodium vacancies as elastic and electric dipole to the elastic and electric fields is not exactly the same in the samples. For example, 180° rotation of an elastic dipole does not lead to a relaxation, while that of an electric dipole does [80,81].

Fig. 12 shows the normalized plot of M''/M''_{max} versus f/f_{max} of the modulus for sample ZnO:1%Na at different temperatures. The observed broad peak is assigned to the summation of relaxations occurring in the bulk materials. The approximate overlap of the modulus curves for all temperatures indicates the dynamical processes occurring at different frequencies are independent of temperature [82].

4. Conclusion

ZnO:Na NPs were prepared by sol–gel technique. Structural, electric and dielectric properties of the prepared samples are investigated. The XRD analysis shows that the NPs are polycrystalline with hexagonal wurtzite structure. Nyquist plots show a non Debye relaxation and the equivalent circuit is a parallel resistor, capacitor and constant phase element. The study of dc conductivity confirms that this later is thermally activated and its variation, at fixed temperature (T = 400 °C), with Na content record sharp diminution which is at the origin of the formation of Na_{Zn} acceptor and estimated to be of p-type for the sample ZnO:1.5%Na. The values of activation energy determined from the slopes of the plots $\log\sigma_{dc}$ versus $1/T$ indicate that the conductivity is ionic. AC conductivity of the prepared samples was found to increase with increase in frequency and complex impedance analysis showed single circular arc type behavior, suggesting the dominance of grain boundary resistance in all the samples. The ac conductivity is analyzed using Jonscher's power law and shows a typical behavior of ionic conductors. The variation of dielectric constant with temperature and frequency indicates a Debye-type dielectric dispersion. The dielectric loss records at high frequencies low values indicating the good quality of the produced powders, property which seems essential in the application of nonlinear optical materials. The variation of the imaginary part of M^* as a function of angular frequency represents one relaxation peak and low values of M'' at low frequencies suggest the suppression of the electrode effect. The observed properties show that Na doped ZnO NPs are very useful for different electronics and sensor applications. Finally, while there are numerous reports on the linear optical properties of ZnO nanostructures, much work remains to be done on studying their nonlinear properties.

References

[1] T.K. Gupta, J. Am. Ceram. Soc. 73 (1990) 1817–2177.
[2] Z. Zhou, K. Kato, T. Komaki, M, Yoshino, H. Yukawa, M. Morinaga, J. Am. Ceram. Soc. 24 (2004) 139–149.
[3] J.H. Lim, C.K. Kang, K.K. Kim, I.K. Park, D.K. Hwang, S.J. Park, Adv. Mater. 18 (2006) 2720–2724.
[4] D.M. Bagnall, Y.F. Chen, Z. Zhu, T. Yao, S. Koyama, M.Y. Shen, T. Goto, Appl. Phys. Lett. 70 (1997) 2230–2232.
[5] G. Srinivasan, R.T. Rajendra Kumar, J. Kumar, Opt. Mater. 30 (2007) 314–317.
[6] S. Ilican, Y. Caglar, M. Caglar, F. Yakuphanoglu, Physica E 35 (2006) 131–138.
[7] E . Fortunato, P . Barquinha, A . Pimentel, A . Goncalves, A . Marques, L Pereira, R. Martins, Thin Solid Films 487 (2005) 40–48.
[8] B.B. RAO, Mater. Chem. Phys. 64 (2000) 62–65.
[9] C. Liu, F. Yun, H. Morkoc, Mater. Electron. 16 (2005) 555–597.
[10] K. Matsubara, P. Fons, K. Iwata, A. Yamada, K. Sakurai, H. Tampo, S. Niki, Thin Solid Films 431 (2003) 16–21.
[11] J.R. Macdonald, Ann. Biomed. Eng. 20 (1992) 289–305.
[12] P. Knauth, J. Schoonman, Electron. Mater.: Sci. Technol. 7 (2002) 111–131.
[13] T. Tsuchiya, N. Yoshimua, Mater. Sci. 24 (1989) 493–499.
[14] S.A. Ansari, A. Nisar, B. Fatma, W. Khan, M. Chaman, A. Azam, A.H. Naqvi, Mater. Res. Bull. 47 (2012) 4161–4168.
[15] R. Kumara, N. Khare, Thin Solid Films 516 (2008) 1302.
[16] H.W. Zhang, Z.R. Wei, Z.Q. Li, G.Y. Dong, Mater. Lett. 61 (2007) 3605.
[17] A. Boukhachem, B. Ouni, M. Karyaoui, A. Madani, R. Chtourou, M. Amlouk, Mater. Sci. Semicond. Proc. 15 (2012) 282–292.
[18] N. Chandel, N. Mehta, A. Kumar, Curr. Appl. Phys. 12 (2012) 405–412.
[19] I.K. Naik, T.Y. Tien, Phys. Chem. Solids 39 (1978) 311–315.
[20] A. Durán, E. Verdin, R. Escamilla, F. Morales, R. Escudero, Mater. Chem. Phys. 133 (2012) 101–120.
[21] C.A. Barbosa, J.M. Henriques, E.L. Albuquerque, V.N. Freire, Phys. Lett. A 372 (2008) 3725–3728.
[22] D.K. Shukla, S. Mollah, Indian J. Pure Appl. Phys. 45 (2007) 52–56.
[23] V.H. Mudavakkat, M. Noor-A-Alam, K. Kamala Bharathi, S. AlFaify, A. Dissanayake, A. Kayani, C.V. Ramana, Thin Solid Films 519 (2011) 7947–7950.
[24] H. El Mkami, B. Deroide, R. Backov, J.V. Zanchetta, Phys. Chem. Solids 61 (2000) 819–826.
[25] M. Cutroni, M. Federico, A. Mandanici, P. Mustarelli, C. Tomasi, Solid State Ionics 681 (1998) 113–115.
[26] Wiem Bousslama, Brigitte Sieber, Habib Elhouichet, Bernard Gelloz, Ahmed Addad, Mokhtar Ferid, J. Phys. D: Appl. Phys. 46 (505104) (2013) 1–8.
[27] Wiem Bousslama, Habib Elhouichet, Bernard Gelloz, Brigitte Sieber, Ahmed Addad, Myriam Moreau, Mokhtar Ferid, Nobuyoshi Koshida, Jpn. J. Appl. Phys. 51 (2012) 04DG13 1-6.
[28] H.B. Liu, X.H. Pan, J.Y. Huang, H.P. He, Z.Z. Ye, Thin Solid Films 540 (2013) 53–57.
[29] D. Wang, S. Gao, J. Alloys Comp. 476 (2009) 925–928.
[30] S.S. Lin, J.G. Lu, Z.Z. Ye, H.P. He, X.Q. Gu, L.X. Chen, J.Y. Huang, B.H. Zhao, Solid State Commun. 148 (2008) 25–28.
[31] P. Bonneau, O. Garnier, G. Calvarin, E. Husson, J.R. Gahvarri, A.W. Hewat, A. Morrel, Solid State Chem. 91 (1991) 350–361.
[32] J. Liu, C.G. Duan, W.G. Yin, W.N. Mei, R.W. Smith, J.R. Hardy, Chem. Phys. 119 (2003) 2812–2819.
[33] W.H. Mulder, J.H. Sluyters, T. Pajkossey, L. Nyikos, Electro-Anal. Chem. 285 (1990) 103–115.
[34] S. Komornicki, M. Radecka, M. Rekas, Mater. Sci. 12 (2001) 11–16.
[35] J.B. Jorcin, M.E. Orazem, N. Pebere, B. Tribollet, Electrochim. Acta 51 (2006) 1473–1479.
[36] N. Sdiri, H. Elhouichet, B. Azeza, F. Mokhtar, J. Non-Cryst. Solids 371–372 (2013) 22–27.
[37] M. Haibado, B. Louati, F. Hlel, K. Guidara, J. Alloys Comp. 509 (2011) 6083–6089.
[38] J. Fan, R. Freer, Appl. Phys. 77 (1995) 4795–4800.
[39] T.K. Gupta, A.C. Miller, Mater. Res. 3 (1988) 745–754.
[40] D.J. Blinks, R.W. Grimes, J. Am. Ceram. Soc. 76 (1993) 2370–2372.
[41] S.T. Kuo, W.H. Tuan, J. Shieh, S.F. Wang, J. Eur. Ceram. Soc. 27 (2007) 4521–4527.
[42] Z. Zhou, K. Katoa, T. Komakia, M. Yoshinoa, H. Yukawaa, M. Morinagaa, K. Moritaal, J. Eur. Ceram. Soc. 24 (2004) 139–146.
[43] T. Larbi, B. Ouni, A. Boukachem, K. Boubaker, M. Amlouk, Mater. Sci. Semicond. Proc. 22 (2014) 50–58.
[44] B. Demirselcuk, V. Bilgin, Appl. Surf. Sci. 273 (2013) 478–483.
[45] M.L. Dinesha, H.S. Jayanna, S. Ashka, G.T. Chandrapp, Optoelectr. Adv. Mater. 11 (2009) 964–969.
[46] G.W. Tomlins, J.L. Routbort, T.O. Mason, J. Appl. Phys. 87 (2000) 117–123.
[47] R. Kumar, N. Khare, Thin Solid Films 516 (2008) 1302–1307.

[48] D.J. Goyal, C. Agashe, M.G. Takwale, V.G. Bhide, J. Mater. Res. 8 (1993) 1052–1056.
[49] B. Choi, H.B. Im, Thin Solid Films 193&194 (1990) 712–720.
[50] S.S. Lin, J.L. Hung, P. Sajgalik, Mater. Sci.: Mater Electron 185 (2004) 254–263.
[51] J. Lü, K. Huang, J. Zhu, X. Chen, X. Song, Z. Sun, Physica B 405 (2010) 3167–3171.
[52] Jian-Jhong Lai, Yow-Jon Lin, Ya-Hui Chen, Hsing-Cheng Chang, Chia-Jyi Liu, Yi-Yan Zou, Yu-Tai Shih, Meng-Chieh Wang, J. Appl. Phys. 110 (2011) 013704–013707.
[53] B. Sundarakannan, K. Kakimoto, H. Ohsato, J. Appl. Phys. 94 (2003) 5182–5187.
[54] Y.S. Yang, J.H. Cho, S.J. Kim, J.E. Kim, H.W. Choi, Y.H. Rim, Phys. Chem. B 108 (2004) 16659–16663.
[55] R.M. Hill, A.K. Jonscher, J. Non-Cryst. Solids 32 (1979) 53–69.
[56] N.F. Mott, E.A. Davis, Electron. Processes Non-Cryst. Mater. (1979) 157–164.
[57] B. Louati, F. Hlel, K. Guidara, J. Alloys Comp. 486 (2009) 299–303.
[58] C.A. Angell, Solid State Ionics 9–10 (1983) 3–741.
[59] V. Biju, M.A. Khadar, Mater. Sci. 38 (2003) 4055–4066.
[60] S. Kurien, J. Mathew, S. Sebastian, S.N. Potty, K.C. George, Mater. Chem. Phys. 98 (2006) 470–476.
[61] K. Funke, Solid State Ionics 94 (1997) 27–33.
[62] A.P. Barranco, M.P. Gutierrez-Amador, A. Huanosta, R. Valenzuela, Appl. Phys. Lett. 73 (1998) 2039–2041.
[63] S.R. Elliot, Philos. Mag. B 37 (1978) 553–560.
[64] S.R. Elliot, Adv. Phys. 36 (1987) 135–217.
[65] A.R. Long, Adv. Phys. 31 (1982) 553–637.
[66] A.R. James, C. Prakash, G. Prasad, J. Phys. D: Appl. Phys. 39 (2006) 1635–1641.
[67] K.S. Cole, R.H. Cole, Chem. Phys. 9 (1941) 341–352.
[68] L. Murawski, R.J. Barczynski, J. Non-Cryst. Solids 185 (1995) 84–93.
[69] N. Sdiri, H. Elhouichet, H. Dhaou, F. Mokhtar, Spectrochim. Acta Part A; Mol. Biomol. Spectrosc. 117 (2014) 309–314.
[70] A. Awadhia, S. Patel, K. Agrawal, S.L. Prog, Cryst. Growth Charact. Mater. 52 (2006) 61–68.
[71] K. Srilatha, K. Sambasiva Rao, Y. Gandhi, V. Ravikumar, N. Veeraiah, J. Alloys Comp. 507 (2010) 391–398.
[72] B. Louati, K. Guidara, M. Gargouri, J. Alloys Comp. 472 (2009) 347–351.
[73] A. Langar, N. Sdiri, H. Elhouichet, M. Ferid, J. Alloys Comp. 590 (2014) 380–387.
[74] A.A. ElBellihi, W.A. Bayoumy, E.M. Masoud, M.A. Mousa, Bull. Korean Chem. Soc. 33 (2012) 2949–2954.
[75] J.B. Charles, F.D. Ganam, Cryst. Res. Technol. 29 (1994) 707–712.
[76] N. Kanagathara, N.G. Renganathan, M.K. Marchewka, N. Sivakumar, K. Gayathri, P. Krishnan, S. Gunasekaran, G. Anbalagan, Spectrochim. Acta A 101 (2013) 112–118.
[77] F.S. Howell, R.A. Bose, P.B. Macedo, C.T. Moynihan, Phys. Chem. 78 (1974) 639–648.
[78] K. Praveen, B. Banarji, V. Srinivas, R.N.P. Choudhary, Res. Lett. 10 (2008) 1–5.
[79] R.N.P. Choudhary, D.K. Pradhan, C.M. Tirado, G.E. Bonilla, R.S. Khatiyar, Mater. Sci. 42 (2007) 7423–7432.
[80] Q.F. Fang, F.J. Liang, X.P. Wang, G.G. Zhang, Z.J. Cheng, Mater. Sci. Eng. A 442 (2006) 43–48.
[81] Q.F. Fang, X.P. Wang, G.G. Zhang, Z.J. Cheng, Phys. Status Solidi (A) 202 (2005) 1041–1047.
[82] G.E. ElFalaky, O.W. Guirguis, N.S. Abd El-Aal, Prog. Nat. Sci.: Mater. Int. 22 (2012) 86–93.